PHOTONIC SENSORS / Vol. 16, No. 1, 2026: 9560010

Review of DAS for Monitoring Industrial Infrastructures

Lang XIE, Juxiang QIU, Hechao WANG, Haitao HUANG,
Shibo HAN, Huicong PENG, Huijuan WU*, and Yu WU*

Key Laboratory of Optical Fiber Sensing & Communications (Ministry of Education of the People's Republic of China), University of Electronic Science and Technology of China, Chengdu 611731, China

*Corresponding authors: Yu WU and Huijuan WU E-mails: wuyu@uestc.edu.cn and hjwu@uestc.edu.cn

Abstract: Distributed acoustic sensing (DAS), based on phase-sensitive optical time-domain reflectometry (Φ-OTDR), transforms optical fibers into distributed vibration sensors through Rayleigh backscattering, enabling real-time industrial monitoring with extensive coverage and high spatial resolution. This review systematically presents key advances and industrial applications made by the optical fiber sensing (OFS) group at University of Electronic Science and Technology of China (UESTC), which include a differential-frequency modulation scheme integrated with a polarization-multifrequency diversity fusion algorithm and achieve pε-level strain sensitivity and suppressed signal fading down to 0.1%, enabling high-fidelity and long-distance sensing using low-cost commercial DAS units. Based on the advanced sensing capability, our developed adaptive feature enhancement method combined with an incremental tree classifier achieves the remarkable 96.55% recognition accuracy for ten types of pipeline intrusion events while reducing retraining time by 98.5% and further attains 99.96% accuracy for five major intrusion types in real field deployments. For railway infrastructure monitoring, our RailFusion-DAS framework utilizes existing fiber-optic cables along the railway to precisely identify three typical track defects with the 98.73% accuracy. Furthermore, by implementing time-frequency analysis and a two-dimensional convolutional neural network classifier on an artificial intelligence (AI) hardware accelerator, we realize an on-chip AI-DAS system that achieves 98.7% accuracy in online fault detection for belt conveyor idlers.

Keywords: Distributed optical fiber sensing; phase-sensitive optical time domain reflectometry; distributed acoustic sensing; artificial intelligence; industrial infrastructure monitoring

Citation: Lang XIE, Juxiang QIU, Hechao WANG, Haitao HUANG, Shibo HAN, Huicong PENG, *et al.*, "Review of DAS for Monitoring Industrial Infrastructures," *Photonic Sensors*, 2026, 16(1): 9560010.

1. Introduction

Distributed acoustic sensing (DAS), based on phase-sensitive optical time-domain reflectometry (Φ-OTDR), has revolutionized distributed sensing by converting conventional optical fibers into spatially continuous vibration sensing through Rayleigh backscattering. This approach effectively repurposes telecommunication cables into large-scale acoustic sensing networks, delivering exceptional advantages, such as long-distance coverage, high spatial resolution, real-time passive operation, and strong immunity to electromagnetic interference [1–3]. Consequently, DAS emerged as a critical perceptual layer in the industrial Internet of

Received: 18 November 2025 / Revised: 22 January 2026

DOI: 10.26599/PhoS.2026.9560010
Article type: Review

things (IIoT), enabling a broad range of industrial monitoring applications [4–7].

Despite these advantages, the transition of DAS from a specialized instrument to a robust, industrial-grade solution faces several persistent challenges. Beyond general issues such as the massive data volume resulting from high-rate sampling or long-range sensing, polarization- and coherence-induced signal fading, and the reliable real-time identification of weak or overlapping acoustic events under noisy field conditions, practical industrial deployments further impose stringent requirements on system scalability, long-term operational robustness, and cost-effectiveness. Representative field-deployed DAS systems for infrastructure monitoring, such as pipeline monitoring and transportation safety [8–10], have demonstrated technical feasibility and sensing coverage; however, they often rely on high-bandwidth data acquisition, complex hardware architectures, or application-specific parameter tuning, which limits their adaptability across heterogeneous industrial scenarios and constrains large-scale deployment.

To mitigate these limitations, extensive research efforts from both academia and industry have been reported in recent years, focusing on advanced signal denoising [11–13], deep learning-based methods for signal enhancement [14, 15], event detection, and classification [16], as well as multi-parameter sensing and data fusion strategies that combine acoustic, strain, and temperature information [17, 18]. These representative advances have substantially improved sensing performance in specific dimensions or application contexts; nevertheless, most existing approaches often incur increased system complexity, high computational overhead, or dependence on large-scale labeled datasets. As a result, a unified system-level framework that jointly balances data efficiency, sensing robustness, and application-driven requirements remains an open challenge, particularly for long-distance and real-time monitoring of critical industrial infrastructures.

In this context, this review systematically presents the differential frequency DAS (DF-DAS) system developed by our group, along with its targeted solutions to these challenges. We first introduce the core principles and technical innovations of DF-DAS, including a differential-frequency modulation scheme that significantly reduces the data volume and a polarization-multifrequency diversity fusion (PMDF) algorithm that suppresses signal fading down to 0.1%, while achieving pε-level strain sensitivity. These foundational advances enable high-fidelity acoustic sensing over long distances using low-cost commercial hardware.

Building on this sensing platform, we demonstrate a suite of industrial applications tailored to domain-specific monitoring requirements: 1) intrusion detection along oil and gas pipelines, integrating adaptive feature enhancement method with an incremental tree classifier to recognize ten types of intrusion events with 99.55% accuracy and a 98.5% reduction while in retraining time; 2) integrated railway monitoring using a RailFusion-DAS framework that identifies multiple track defects with 98.73% accuracy by leveraging existing trackside fiber cables; 3) real-time fault diagnosis of belt conveyor idlers via field-programmable gate array (FPGA)-accelerated AI-DAS system, achieving 98.7% online classification accuracy with low power consumption.

This review not only outlines the architecture and performance of these implementations but also discusses the remaining challenges and emerging research prospects. It is our expectation that this work will provide a valuable reference for researchers and engineers, promoting the broader adoption of intelligent DAS-based monitoring across industrial infrastructures.

2. Principles and techniques of DF-DAS

2.1 DF-DAS for data under-sampling

Conventional Φ-OTDR based DAS systems, stemming from early coherent detection schemes [19], impose stringent demands on data acquisition (DAQ) performance, resulting in high computation load for demodulation, transmission, and storage. To alleviate these issues, multiple strategies, including wavelet-curvelet-based signal compression [20], under-sampling [21], and reduced sampling resolution [22], have been proposed. However, these approaches offer only partial relief, as underlying requirements for wide detection bandwidths and high data throughput remain unaddressed [23].

To overcome these inherent limitations, we propose a DF-DAS architecture that strategically shifts the signal to an intermediate frequency by applying secondary modulation to the local oscillator (LO), as depicted in Fig. 1(a) [24]. Specifically, the detection pulse and the LO are independently frequency-shifted by two acousto-optic modulators (AOMs), and coherent mixing at the balanced photodetector yields an electrical beat signal determined by the difference between the two frequency shifts. For the alternating current (AC) component after balanced detection, the beat signal can be expressed as

$$I(t)=2E_lE_r\sum_{i=1}^{M}r_i\mathrm{rect}\left[\left(t-\tau_i\right)/W\right]\times \cos\left[2\pi\left(\left|f_1-f_2\right|\right)+\varphi(t)\right] \quad (1)$$

where E_l and E_r denote the electric field amplitudes of the LO and the Rayleigh backscattered signal, respectively; r_i and τ_i are the amplitude coefficient and relative delay of the i-th scattering center; M is the total number of scattering centers within the probe pulse width W; f_1 and f_2 represent the frequency shifts induced by AOM_1 (probe pulse) and AOM_2 (LO), respectively; $\varphi(t)$ denotes the phase variation induced by external perturbations.

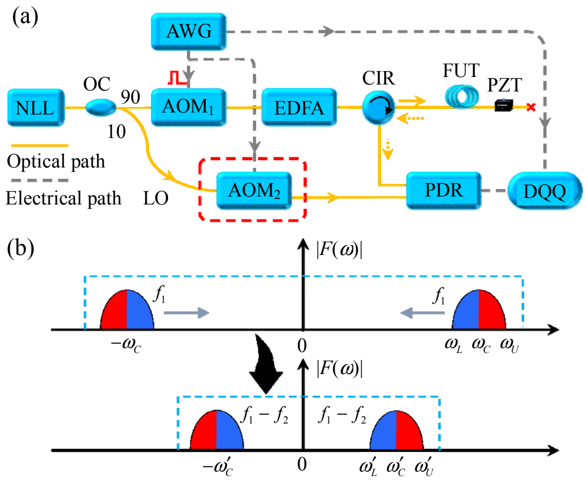

Fig. 1 DF-DAS system: (a) DF-DAS experimental setup and (b) the principle of differential frequency modulation.

Equation (1) explicitly shows that, after coherent mixing, the Rayleigh backscattered signal is translated into the electrical domain and modulated onto a carrier centered at the differential frequency $|f_1-f_2|$, while the disturbance-induced $\varphi(t)$ is preserved. This frequency-shifted LO generates a low-frequency beat signal, as shown in Fig. 1(b), which substantially relaxes the requirements on the sampling rate and system bandwidth without compromising demodulation precision, thereby paving the way for cost-effective and scalable DAS implementation.

Experimental validation confirms that the DF-DAS system retains the fidelity of the conventional DAS demodulation, while reducing the data volume and latency by approximately 75%. For a 61 km FUT, the reduced frequency shift enables the minimum acquisition rate to decrease from 160 MSa/s in the conventional DAS to 40 MSa/s in the DF-DAS, resulting in a fourfold reduction in the raw data volume per 1-s acquisition window. Correspondingly, under identical hardware and software conditions, the phase demodulation time is reduced from 36.8 s to 8.34 s, confirming a fourfold improvement in processing latency. Thus, the DAQ bandwidth and storage constraints are effectively relaxed, enabling a compact and scalable sensing solution suited to long-distance applications.

In conclusion, the DF-DAS establishes a cost-effective and practical architecture for the coherent DAS, enabling large-scale, long-term, and high-fidelity monitoring of critical infrastructures such as pipelines and railways.

2.2 DF-DAS fading suppression with PMDF

Despite the significant reductions in the bandwidth and data volume archived by the DF-DAS, the system remains susceptible to signal fading – particularly polarization and coherence fading [25–31] – which degrades phase stability and strain sensitivity. To overcome these limitations, we develop a polarization-multifrequency diversity fusion (PMDF) algorithm [32], as illustrated in Fig. 2. This method integrates polarization and multi-frequency information to enhance signal integrity, effectively suppressing fading during phase demodulation. By dynamically selecting the optimal polarization component and performing diversity-based signal fusion, the PMDF algorithm ensures stable and high-fidelity phase recovery under varying sensing conditions.

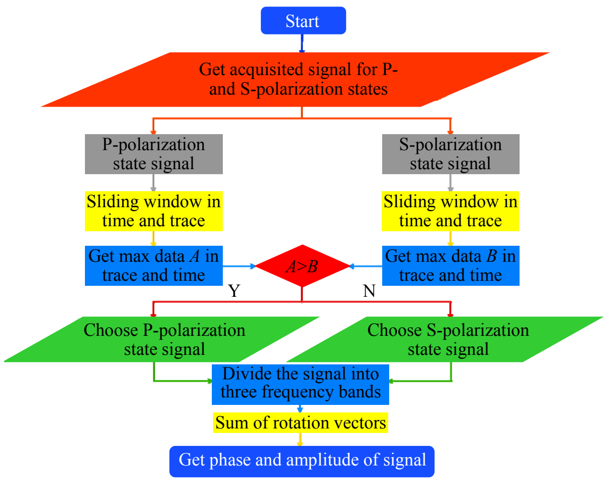

Fig. 2 Flow chart of the polarization-multifrequency diversity fusion algorithm.

The following describes the detailed implementation of the PMDF algorithm. Firstly, the acquired P- and S-polarization signals (obtained from a polarization diversity receiver [33]) are used to construct the signal intensity matrices $\mathbf{P}_{m\times n}$ and $\mathbf{S}_{m\times n}$, respectively, forming an $m\times n$ matrix with dimensions of time (m) and distance (n). Then, a temporal-spatial window $\mathbf{T}_{m'\times n'}$ is selected. $\mathbf{P}_{m\times n}$ and $\mathbf{S}_{m\times n}$ are divided into N equally sized segments based on this window size. For each segment, the minimum signal amplitudes of the P- and S-polarization components are evaluated as quantitative indicators of fading severity. The polarization channel exhibiting the larger minimum amplitude within the window is selected as the optimal channel for subsequent phase demodulation, and the selected polarization signals from different probing frequencies are then coherently fused using a rotated-vector-sum (RVS) methods [34–36] to enhance robustness against frequency-dependent fading while preserving disturbance-induced phase variations. This selection-and-fusion strategy ensures that phase extraction avoids polarization states affected by deep fading, maintains the sufficient signal-to-noise ratio (SNR), and enables stable phase recovery, after which in-phase and quadrature (IQ) demodulation, phase reconstruction, and phase unwrapping are performed to monitor external disturbance events.

Experimental results demonstrate that the PMDF algorithm significantly mitigates both coherence and polarization fading. Compared to the conventional arctangent and RVS, the PMDF markedly reduces phase noise and fading artifacts, achieving a noise floor as low as −61 dB rad^2/Hz and a strain resolution of 30 pε/√Hz. To quantitatively evaluate fading suppression performance, statistical analysis of amplitude distributions is performed over the entire sensing fiber (61 km FUT) using 1 s acquisition windows. A fading event is defined when the instantaneous signal amplitude at a given spatiotemporal sampling point falls below 20% of the mean amplitude [35]. The fading probability is then calculated as the ratio of fading occurrences to the total number of spatiotemporal samples within each acquisition window. Based on this definition, the probability of fading events is reduced to below 0.1% using the PMDF. This result indicates a substantial improvement in robustness and operational stability compared with the conventional phase demodulation methods.

In summary, the PMDF technique provides a highly effective solution for fading suppression, substantially improving the sensitivity, reliability, and stability of DF-DAS systems. These enhancements enable more accurate detection of weak vibration and intrusion signals, support high-fidelity feature extraction, and facilitate early-stage fault diagnosis in long-range distributed sensing applications.

3. DF-DAS for oil and gas pipelines monitoring

The DAS technology has been extensively deployed across the petroleum industry, with established applications in seismic exploration and pipeline integrity monitoring – spanning the full lifecycle from energy extraction to transportation [37–39].

Within pipeline operation, third-party intrusion represents a critical risk factor with potentially severe environmental and safety consequences. Although DAS systems utilizing fiber-optic cables along pipelines enable long-distance vibration monitoring, the transformation of converting raw DAS data into reliable threat identification still faces fundamental challenges: 1) the critical need for fine-grained classification to not only detect but also identify the nature and source of diverse third-party security events; 2) the high similarity of time-frequency signatures among different intrusion types, often masked by complex ambient noise; 3) the demand for recognition models with strong generalization across diverse environments and evolving threats; 4) the stringent latency requirements for real-time safety response.

The DF-DAS system operates with a pulse repetition rate of 1 kHz and a pulse width of 100 ns (corresponding to a spatial resolution of approximately 10 m), together with a monitoring distance exceeding 50 km, which are widely adopted in practical pipeline monitoring systems [55].

The following sections present our targeted solutions to these challenges.

3.1 Noise suppression and feature enhancement with AWTFE

DAS signals are frequently contaminated by electronic noise, signal fading, and environmental disturbances, which collectively degrade recognition performance. To address these issues, we develop an adaptive weighted thresholding and feature enhancement (AWTFE) method that combines median filtering for high-frequency noise suppression with adaptive thresholding and histogram equalization for feature enhancement. Subsequently, a fixed and monotonic pseudo-color mapping is applied to convert the enhanced grayscale images into discriminative red-green-blue (RGB) representations, which increases channel diversity for convolutional neural network (CNN)-based feature extraction while preserving the original intensity ordering, thereby avoiding the introduction of artificial intensity inversions or non-physical feature distortions that may arise from non-monotonic color mappings.

As illustrated in Fig. 3, the AWTFE processing markedly enhances the discriminability of five typical intrusion events. By suppressing noise-induced artifacts and amplifying subtle but physically meaningful signal structures, the AWTFE effectively enlarges the feature margins among highly similar intrusion categories. Evaluations using three classifiers: a two-dimensional convolutional neural network (2D-CNN), a residual network with 18 layers (ResNet18), and VGG13 with batch normalization (VGG13_BN), a 13-layer convolutional network developed by the Visual Geometry Group (VGG). The results demonstrate that the AWTFE increases recognition accuracy by up to 13.45%, with the best model achieving the accuracy of 99.96% (Fig. 4). These results indicate that the AWTFE directly addresses the challenge of high inter-class similarity by enhancing intrinsic feature separability, thereby providing a robust front-end representation for fine-grained and noise-resilient intrusion recognition.

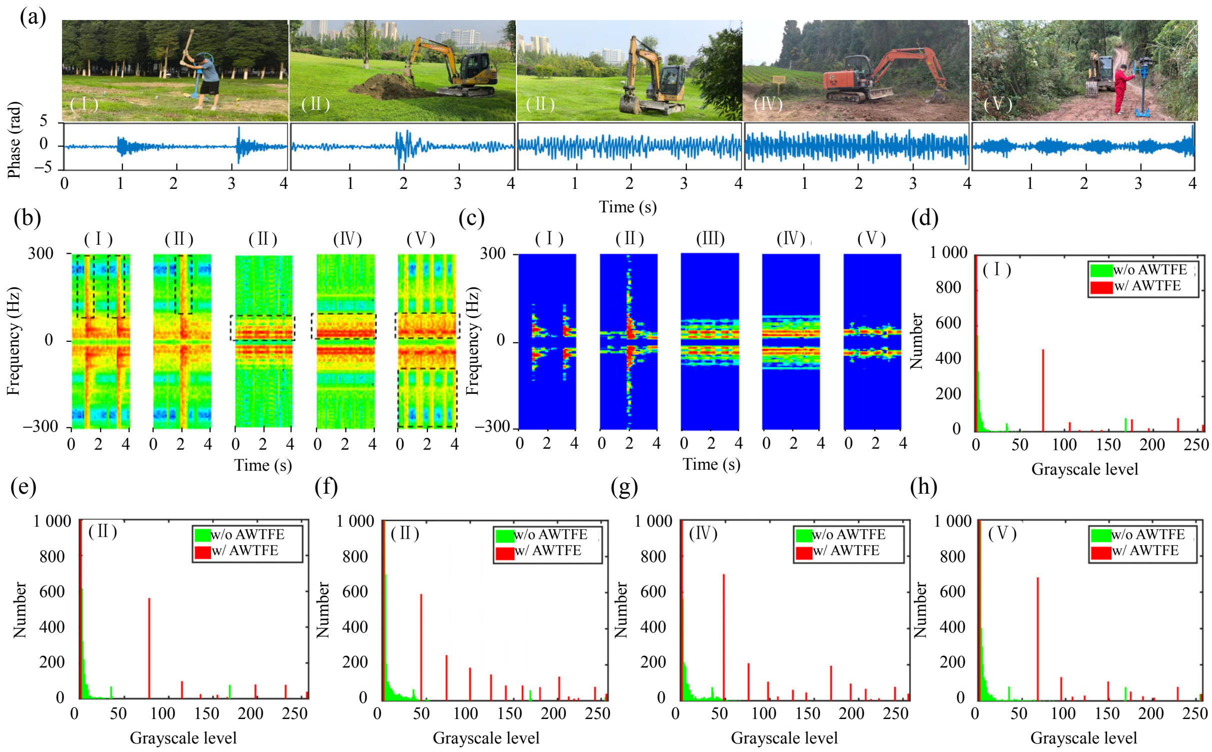

Fig. 3 AWTFE image enhancement [Event (I): manual excavation; Event (II) mechanical excavation; Event (III) excavator idling; Event (IV) tamping machine operation; Event (V) drilling machine operation, respectively]: (a) on-site construction scenes and corresponding time-domain signals for Events (I)–(V), (b) RGB images of typical signals for each event, (c) RGB images after being processed with the AWTFE method, and (d)–(h) histograms of images for Events (I)–(V) with (red curves) and without (green curves) the AWTFE method.

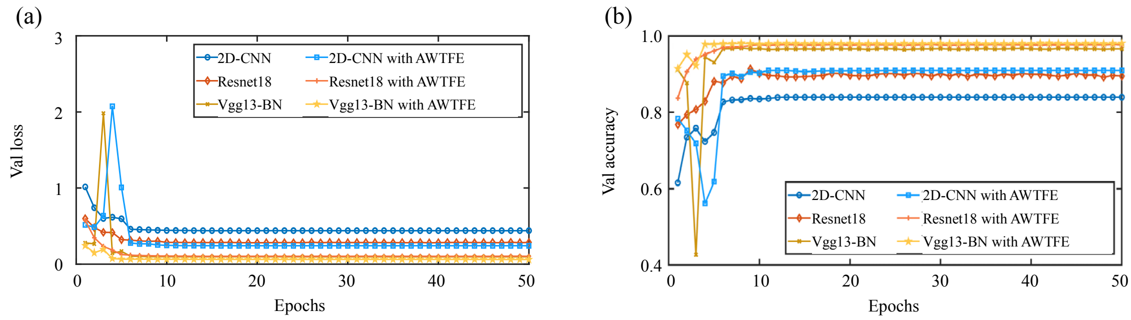

Fig. 4 Convergence curves: (a) loss entropy convergence curve and (b) accuracy convergence curve. Validation results are indicated as "Val loss" and "Val accuracy".

3.2 Incremental fine-grained tree classification

Most existing DAS signal recognition algorithms face two major limitations in pipeline third-party intrusion monitoring. First, achieving fine-grained identification of diverse threat types, such as distinguishing among various mechanical operation, manual digging, and vehicle movements, remains inherently challenging due to high inter-class similarity and environmental variability. Second, existing models lack efficient adaptability to newly emerging intrusion events, often requiring computationally expensive full-model retraining.

These limitations significantly hinder the operational deployment of DAS systems for accurate and continuously evolving threat identification.

To address these challenges, we propose a cross-scene and multi-event recognition framework based on a tree-structured classifier as illustrated in Fig. 5. Our approach employs an encoder-based long short-term memory (LSTM) network to extract discriminative spatiotemporal features from raw DAS signals across varied environments. Subsequently, hierarchical spectral clustering is then applied to construct a feature-aware classification tree, while multi-task learning jointly optimizes all tree nodes to enhance feature separability and classification robustness. Furthermore, the framework integrates an incremental learning mechanism that dynamically assigns newly added event types to optimal non-leaf nodes, enabling efficient model adaptation without full retraining. This integrated solution not only improves fine-grained recognition of complex intrusion events but also maintains high performance across changing field conditions, thereby offering a scalable, adaptive, and computationally efficient solution for real-time pipeline integrity monitoring.

As shown in Fig. 6, field tests across three distinct scenarios demonstrate that our method achieves the classification accuracy of 96.60% for nine common events, validating its capability for fine-grained categorization under complex and variable field conditions. When incorporating an additional event type, the incremental learning model maintains the high accuracy of 96.55% across all ten events, while the required training time amounts to only 1.5% of that required for full model retraining, thereby directly satisfying the low-latency requirement for real-time deployment. Moreover, the hierarchical structure and cross-scene feature learning strategy enhance model generalization across diverse environments and evolving threat patterns. These results collectively demonstrate that the proposed method effectively addresses the key challenges of fine-grained recognition, strong generalization, and real-time adaptability in pipeline intrusion monitoring.

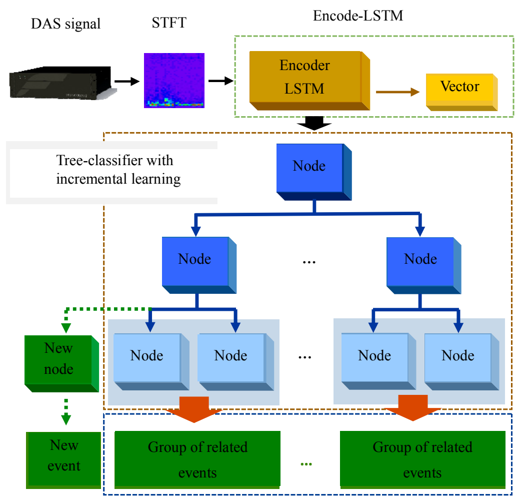

Fig. 5 Cross-scene multi-event recognition flowchart in the fiber-optic DAS.

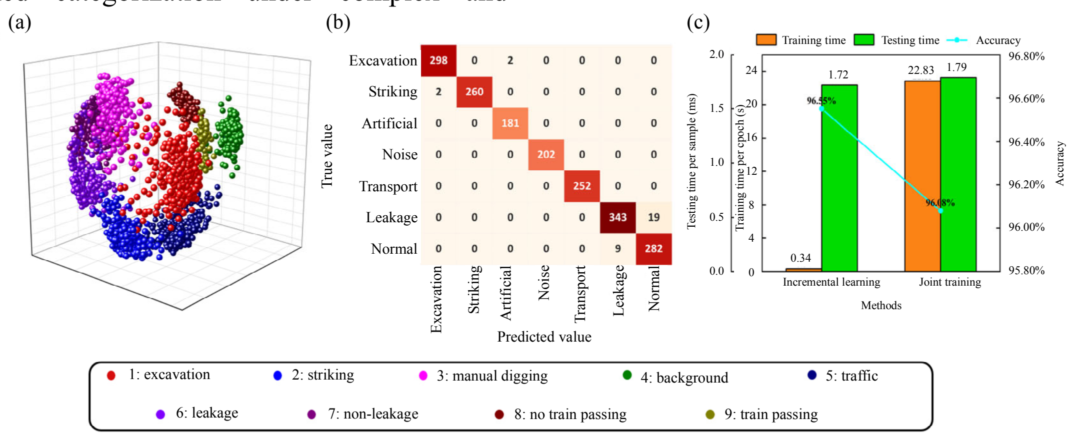

Fig. 6 Recognition performance of the incremental tree classifier: (a) feature distribution of nine intrusion events, (b) confusion matrix for multi-class event identification, and (c) incremental learning result after introducing an additional event type.

4. DF-DAS for railway infrastructures monitoring

Modern railway operations require integrated monitoring solutions capable of simultaneously ensuring operational safety and infrastructure integrity [40–44]. The conventional sensing technologies are not only highly susceptible to electromagnetic interference but also pose significant practical deployment challenges, including the complexity of installing extensive sensor arrays and providing a stable power supply along the entire line [45–50]. In 2014, our group pioneered the use of existing fiber-optic cables along railway tracks for train-induced vibration sensing [45]. This approach first demonstrated the feasibility of real-time train positioning and speed monitoring using pre-deployed telecommunication infrastructure. However, a critical challenge remains in the reliable extraction of weak vibration signals from complex acoustic backgrounds, which is essential for early-stage defect detection.

In railway monitoring scenarios, defect-related vibrations are dominated by low-frequency components, while higher-frequency components suffer pronounced attenuation during structural propagation [51, 52]. Accordingly, the DF-DAS system parameters are set to a pulse width of 100 ns (~10 m spatial resolution) and a pulse repetition rate of 1 kHz.

This section details our enhanced DAS framework, designed to address these challenges and advance the capabilities of railway monitoring, with particular emphasis on weak-signal extraction, robustness under complex acoustic backgrounds, and reliable defect identification under constrained fiber deployment conditions.

4.1 High-precision train positioning and speed estimation

This study implements a dual-model imaging approach to achieve real-time and high-precision train positioning using the DAS. A U-net-based network [Fig. 7(a)] is employed to accurately extract train-induced vibration signals from the background noise, while the you only look once (YOLO) concurrently performs multi-train detection and localization. The integrated algorithm demonstrates robust performance across diverse operational scenarios, including weak signal conditions and multi-train environments [Fig. 7(b)].

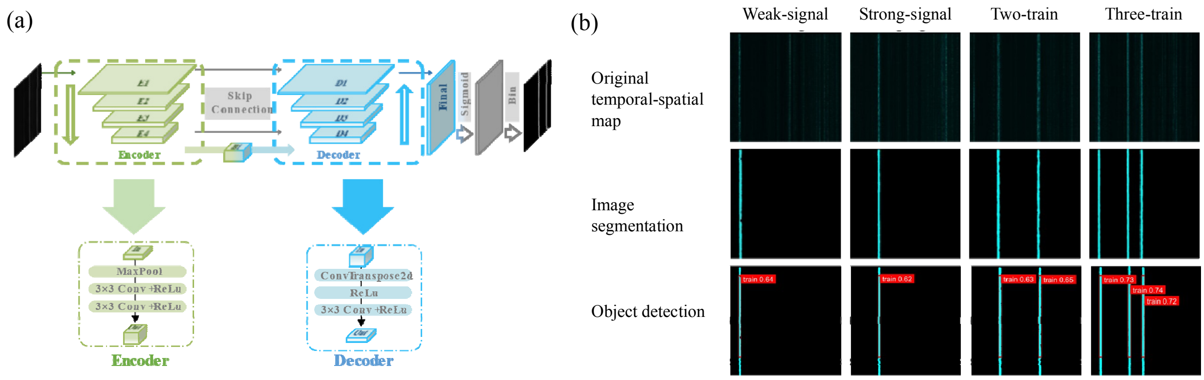

Fig. 7 Illustration of U-net-based DAS signal analysis: (a) the U-net architecture and schematic diagrams of its encoder and decoder modules and (b) image segmentation and object detection on four typical DAS signal types.

The U-net segmentation achieves intersection over union (IoU) and Dice coefficients of 0.87 and 0.92, respectively, substantially outperforming the conventional approaches (Table 1). This precise signal extraction enables reliable train tracking, although inherent signal artifacts can initially cause spurious jumps in localization traces. To address this, a Kalman filter with backtracking suppression is implemented, effectively smoothing positional data and eliminating erroneous movements (Fig. 8).

Comprehensive validation across multiple operational scenarios demonstrates the system's accuracy and robustness (Fig. 9). The integrated method achieves an average localization error of 5.5 m and a velocity estimation error of 0.25 km/h, satisfying practical engineering requirements for railway monitoring. Furthermore, the approach demonstrates consistent performance across varying train speeds and configurations, providing a reliable foundation for subsequent applications in track condition monitoring. By ensuring accurate train-induced vibration extraction and stable kinematic estimation under weak-signal and multi-train conditions, this framework directly addresses the challenges of complex acoustic backgrounds and establishes a prerequisite for reliable downstream defect detection.

Table 1 Comparison of segmentation methods on typical spatiotemporal signals.

Method	IoU	Dice	Note
Threshold segmentation [53]	0.52	0.68	Not sensitive to weak signals
Canny edge detection [54]	0.65	0.76	Susceptible to interference
U-net (our method)	0.87	0.92	High robustness

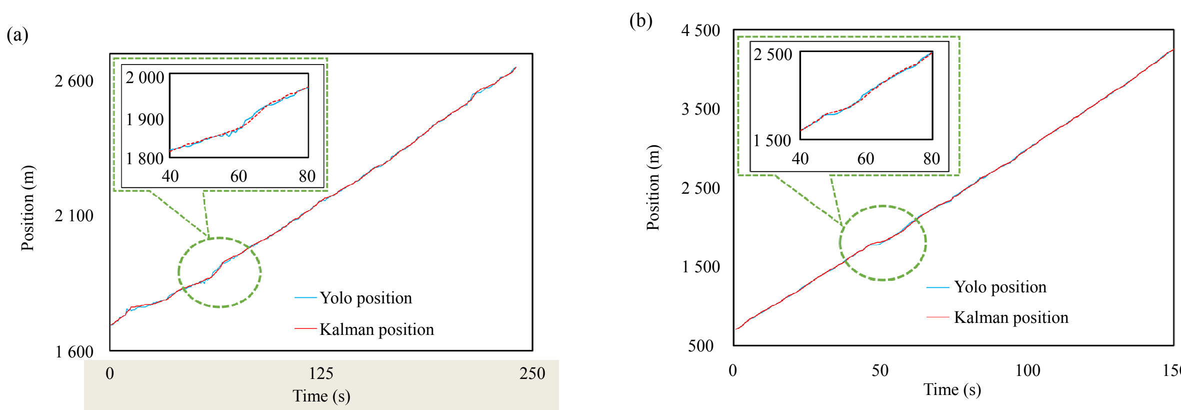

Fig. 8 Comparison of YOLO-based detection and Kalman filtering for train position-time curves: (a) high-speed scenario; (b) low-speed scenario.

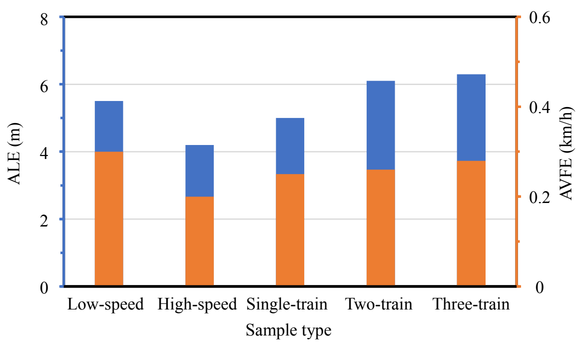

Fig. 9 Comparison of localization and velocity errors for DAS-based trains under different data types (ALE: average localization error; AVEE: average velocity estimation error).

4.2 Track defect identification and classification

4.2.1 Weak signal detection under challenging deployment conditions

Different types of track defects generate distinct vibration patterns: rail corrugation induces periodic vibrations, unsupported sleepers manifest as irregular signal jumps, and rolling contact fatigue (RCF) exhibits localized low-frequency steady-state vibrations. While theoretically identifiable, detecting these patterns under real-world operational conditions remains challenging. DAS signals are influenced by multiple factors, including signal attenuation, environmental noise, and dynamic variations. Crucially, the installation methodology of optical cables – particularly air-filled trench deployment as used in this study – significantly affects signal quality. Our simulation and experimental validation confirm that air-filled trenches provide the poorest signal reception due to acoustic impedance mismatch at the air-trench interface, resulting in consistently lower amplitude and SNRs compared to direct-buried configurations [55].

This suboptimal installation scenario presents a considerable detection challenge: wheel-rail vibrations must propagate through subgrade and soil before reaching the air-filled trench, causing substantial signal reflection and energy loss [56, 57]. The resulting signals suffer from significant attenuation and frequency distortion, while extraneous vibration sources further obscure defect signatures. The conventional spectral analysis proves inadequate under these conditions, necessitating advanced signal processing approaches.

To address these limitations, we develop, for the first time, a unified DAS-based defect recognition framework combining multi-dimensional feature extraction, wavelet-based energy enhancement, and machine learning-driven classification [48] (Fig. 10). The system constructs comprehensive vibration representations by extracting frequency center (FC), frequency variance (FV), and spectral entropy from DAS-measured responses, effectively capturing the distinctive vibration signatures associated with different defect types.

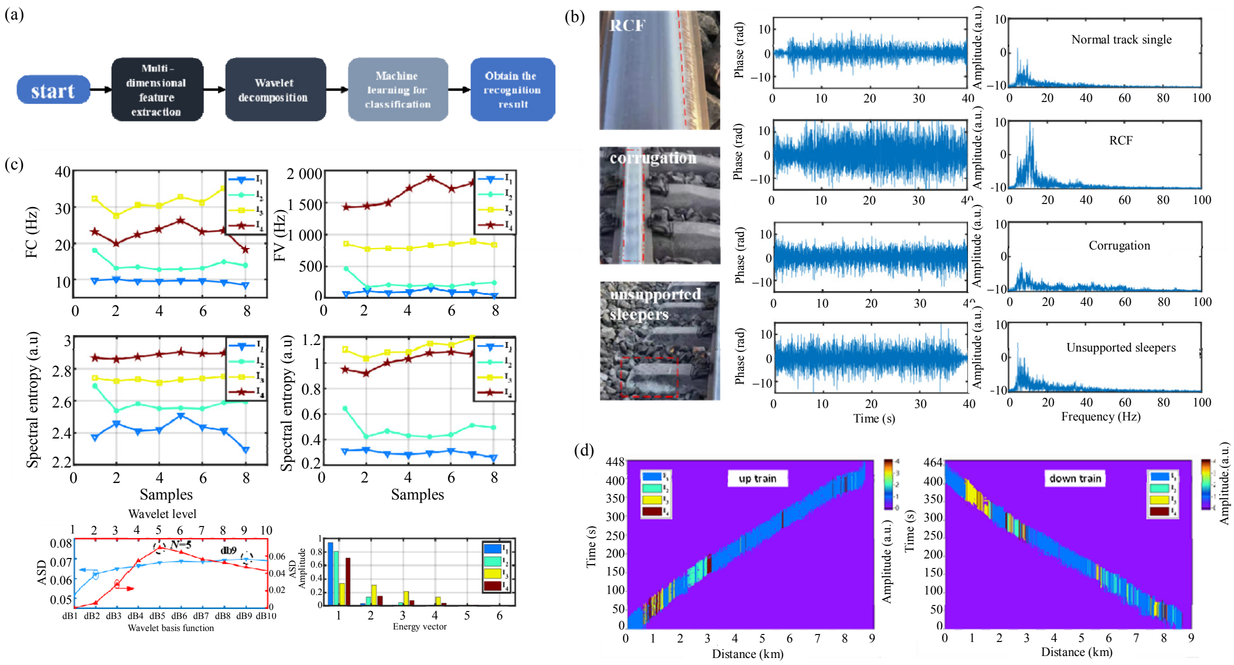

Fig. 10 Overview of the proposed track defect identification system: (a) workflow of the proposed track defect identification system, (b) time-frequency signals of train passages over tracks with different defects, (c) extracted multi-dimensional feature vectors for different defect types, and (d) defect recognition results and validation against field inspection.

Wavelet decomposition refines the energy distribution, emphasizing low-frequency defect components while suppressing high-frequency interference, thereby amplifying subtle structural anomalies in the vibration spectrum. The extracted temporal-spectral features are fused into a unified eigenvector and classified via a Bayesian-optimized support vector machine (SVM), enabling efficient and robust recognition across diverse track conditions.

To verify the distinguishing accuracy of the multi-dimensional eigenvector, a dataset containing four types of characteristic track events is constructed. Each event type includes 2 000 samples, resulting in a total of 8 000 labeled samples. For training, 1 500 samples (75%) per event are randomly selected, while the remaining 500 samples (25%) per event are reserved for testing. This dataset division ensures balanced representation of all event types and supports robust evaluation of the classification framework. Evaluation on this dataset demonstrates the average recognition accuracy of 94.0%, outperforming the one-dimensional CNN (1D-CNN) and the artificial neural network (ANN) models. The predicted defect positions exhibit strong agreement with field inspection benchmarks, confirming the system's reliability in detecting early-stage degradation. Moreover, a further extension using a ResNet34 configuration improves accuracy to 98.6%, highlighting the scalability and adaptability of the approach under varying sensing conditions. These results demonstrate that the proposed framework effectively mitigates the weak-signal challenge induced by suboptimal air-filled trench deployment, enabling reliable early-stage defect detection under severely attenuated sensing conditions.

4.2.2 RailFusion-DAS: multi-kinematic representation with attentional fusion

Although the above framework achieves high recognition accuracy, its performance remains constrained by the limited vibration perception associated with air-filled trench installations. To overcome this constraint and enhance weak-signal sensitivity, we develop RailFusion-DAS [55], as illustrated in Fig. 11, a unified framework that replaces manual feature engineering with multi-kinematic representations and intelligent multi-domain feature learning. The system employs a novel approach to amplify subtle defect characteristics in weak signals through three key innovations.

First, we construct multi-kinematic representations by deriving velocity and acceleration signals from raw displacement measurements via time-domain differentiation. This representation significantly enhances the discriminability of low-frequency defect components that are typically obscured in the conventional displacement-based analysis. The velocity profile amplifies transient features of unsupported sleepers, while acceleration signals emphasize periodic patterns characteristic of rail corrugation. Second, parallel temporal and spectral processing branches capture complementary defect characteristics across domains. The temporal branch extracts time-domain features, including variance and sample entropy, while the spectral branch analyzes frequency center and power spectrum entropy. This dual-domain approach ensures comprehensive characterization of defect signatures. Third, an attention-based fusion mechanism dynamically weights and integrates multi-dimensional features to enhance defect-related patterns. The attention module selectively emphasizes the most discriminative features from both domains, effectively suppressing irrelevant noise components and amplifying subtle defect indicators.

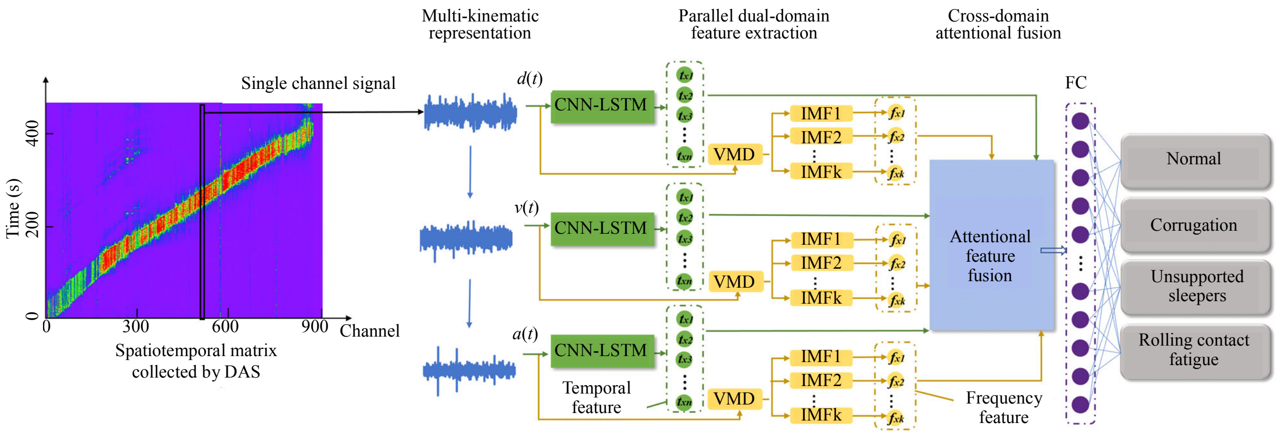

Fig. 11 Multi-dimensional information extraction and fusion for railway defect identification.

Experimental validation on a dataset of 9 481 samples demonstrates exceptional performance. The samples are obtained by segmenting vibration signals into 5-s intervals and are categorized into four classes: normal (3 269 samples), corrugation (1 205 samples), unsupported sleepers

(1 523 samples), and RCF (3 484 samples). The dataset is divided into training and test sets with a 7:3 ratio (6 636 training samples and 2 845 test samples). As shown in Fig. 12, the RailFusion-DAS achieves the defect detection accuracy of 98.73%, with precision, recall, and F1-scores all exceeding 96% across all defect categories. The framework significantly outperforms established benchmarks, including SVM [39], CNN [58], and ResNet [59] approaches. Error analysis reveals that misclassifications primarily occur between mechanistically similar defects, confirming the system's logical consistency in distinguishing defect types based on their physical characteristics. This integrated approach demonstrates that sophisticated feature extraction and fusion can overcome the limitations of suboptimal fiber deployment and weak vibration perception, thereby directly addressing the challenges of weak defect signatures, high inter-defect similarity, and complex operational noise. This study advances integrated railway surveillance by merging DAS-based train monitoring with track defect diagnosis.

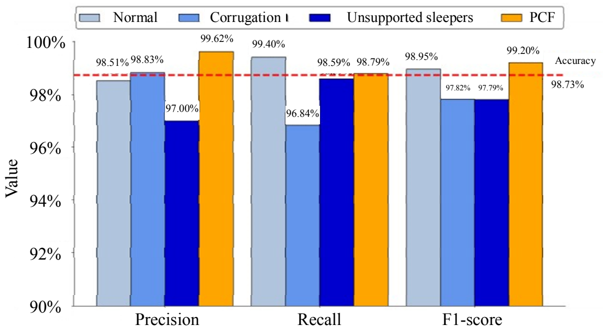

Fig. 12 RailFusion-DAS performance test results.

5. DF-DAS for belt conveyor monitoring

Belt conveyors, as critical infrastructure for bulk material handling, require continuous monitoring to ensure operational safety and prevent costly failures, such as belt misalignment and tearing. The traditional methods relying on localized sensors and periodic maintenance lack the distributed coverage necessary for early fault detection. The distributed sensing capability of the DAS, combined with embedded intelligence, offers a transformative solution for predictive maintenance in industrial environments [60, 61].

We implement a comprehensive monitoring system using a vibration-sensitive armored sensing cable deployed along a 500-m conveyor section (Fig. 13). The system captures synchronized vibration data along the entire conveyor line, enabling real-time condition monitoring of idlers and other critical components. Considering the characteristic vibration signatures of idler defects, which are typically dominated by localized and relatively high-frequency components [62], the DF-DAS system parameters are set to a pulse repetition rate of 10 kHz and a spatial resolution of 5 m, allowing effective localization and detection of idler-related anomalies along the conveyor.

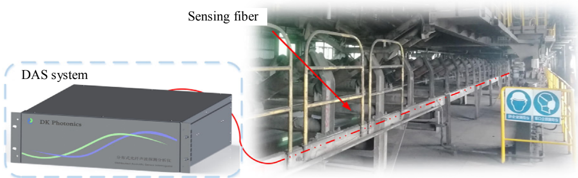

Fig. 13 Schematic of the belt conveyor monitoring with the DAS.

Figure 14 presents the time-frequency representations of three representative event types: background noise (Type 0), mild idler fault (Type 1), and severe idler fault (Type 2). Clear spectral distinctions are observed among the categories, where mild and severe faults exhibit progressively enhanced broadband energy and richer harmonic components relative to the stable background state. These discriminative spectral features enable the FPGA-deployed 2D-CNN to effectively extract and classify fault signatures in real time.

Figure 15 illustrates the confusion matrix and quantitative performance metrics of the trained model. The system achieves the overall classification accuracy of approximately 98.7%, with precision and recall exceeding 97% across all fault categories. Notably, even under the strong background noise, the FPGA implementation maintains stable inference accuracy, demonstrating the robustness of the feature learning process and the efficiency of on-chip parallel computing.

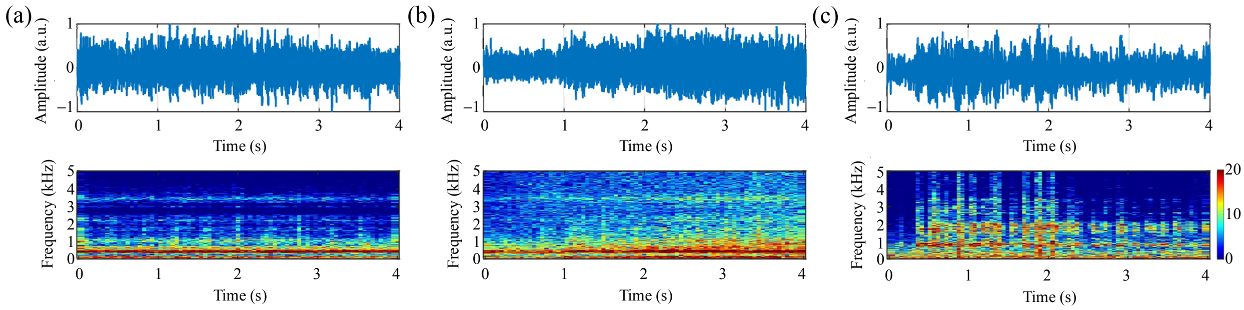

Fig. 14 Time-domain and corresponding short-time Fourier transform (STFT) spectra for three representative event types: (a) background noise (Type 0), (b) mild idler fault (Type 1), and (c) severe idler fault (Type 2). Each case presents a 4 s segment of DAS data, which serves as the recognition window length for the trained model. The color bar indicates the STFT magnitude in dB (rad^2/Hz).

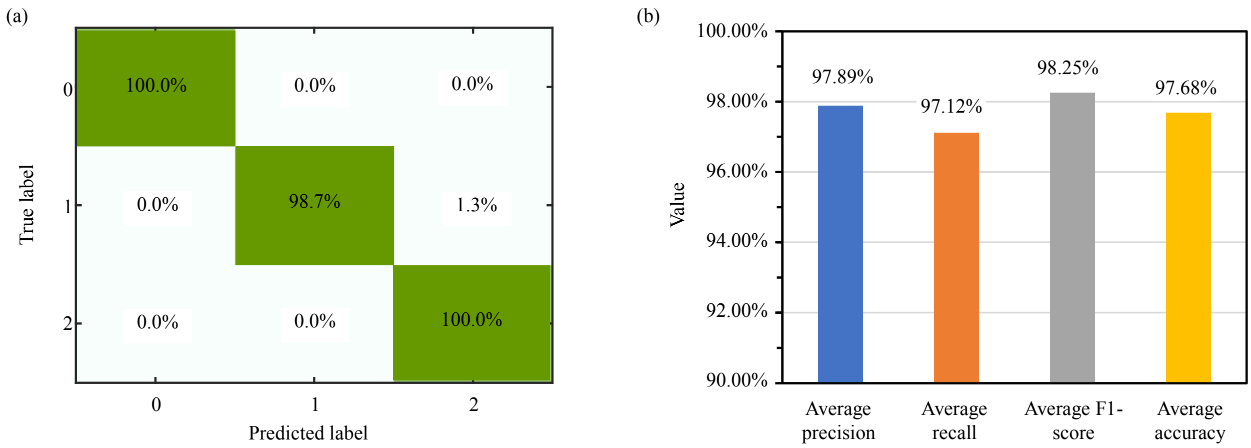

Fig. 15 Evaluation of idler fault recognition accuracy: (a) confusion matrix for the real-field test, where rows indicate predicted labels and columns indicate true labels (0: background noise; 1: mild idler fault; 2: severe idler fault) and (b) corresponding performance metrics including average precision, recall, F1-score, and accuracy.

To overcome the high computational load and latency associated with centralized processing, the 2D-CNN classifier is optimized and deployed on a Zynq UltraScale+MPSoC ZCU102 FPGA platform using the Vitis-AI toolchain. As shown in Fig. 16, in the FPGA-based AI-DAS processing pipeline [63], the STFT preprocessing and deep learning model are quantized to INT8 precision, reducing computational complexity while maintaining classification accuracy comparable to that of central processing unit (CPU)-based inference, with only negligible quantization-induced degradation.

On the FPGA, the system achieves the average inference time of only 0.398 ms per sensing node. With a total fiber length of 500 m and a spatial resolution of 2 m, the entire line could be processed in real time, whereas CPU-based host processing typically suffers from higher latency and data transfer overheads in long-range DAS applications. As a result, the proposed FPGA implementation significantly outperforms the conventional CPU-based solutions in both speed and power efficiency. The FPGA-based AI-DAS system consumes only 25 W, demonstrating a 49× improvement in energy efficiency over desktop CPUs.

This integrated AI-DAS system exemplifies a successful transition from time-based to condition-based maintenance in industrial environments. It reliably identifies early mechanical faults through high-frequency vibration signatures, even under strong ambient noise. By combining distributed fiber sensing with FPGA-accelerated edge intelligence, the system provides a scalable, low-power, and high-speed monitoring solution suitable for long-distance conveyors and other critical infrastructure. This case serves as a reference implementation for embedding lightweight AI models within edge devices, enabling real-time, reliable, and energy-efficient fault diagnosis.

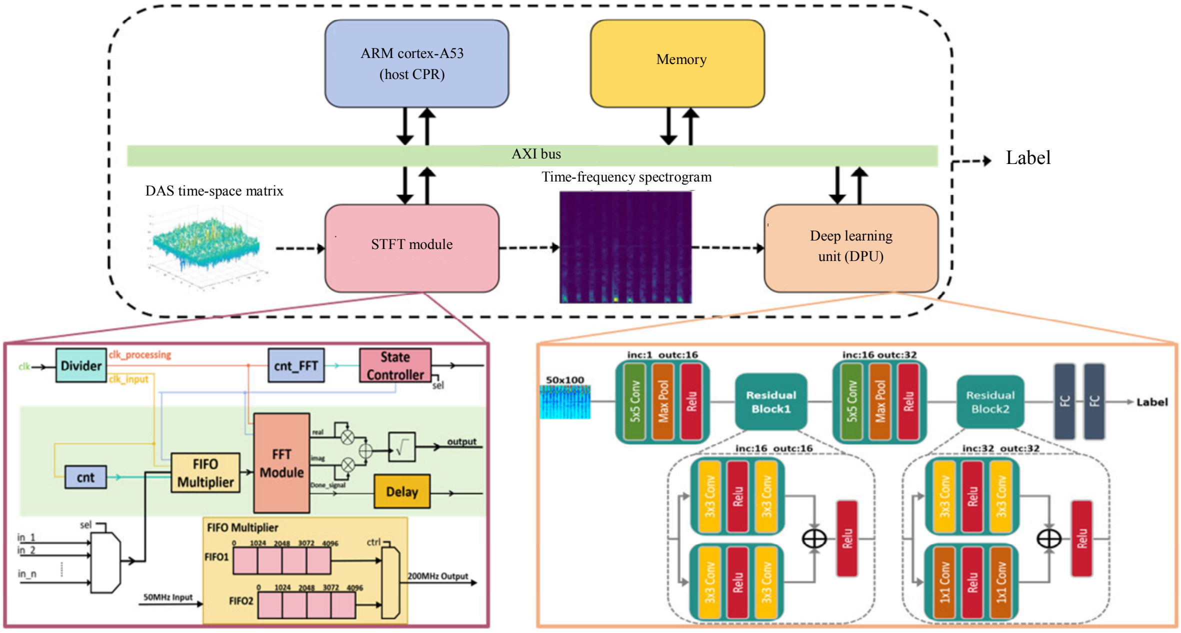

Fig. 16 FPGA-based AI-DAS processing pipeline.

6. Conclusions

Leveraging its unique capabilities, including long-range coverage, high spatial resolution, and the reuse of existing optical fiber infrastructures, the DAS is transitioning from a specialized instrument into a pervasive layer in the IIoT. This review has presented a series of innovations developed by the UESTC optical fiber sensing (OFS) group, spanning multiple industrial monitoring scenarios: 1) the DF-DAS system achieves pε-level strain sensitivity and suppresses signal fading down to 0.1%, providing a high-fidelity sensing foundation; 2) a pipeline intrusion recognition framework combining adaptive feature enhancement and incremental fine-grained learning tree attains 96.55% accuracy for ten event types while reducing retraining time by 98.5%; 3) the RailFusion-DAS system enables accurate diagnosis of multiple track defects with 98.73% accuracy using existing trackside fibers; 4) an FPGA-accelerated AI-DAS system realizes real-time fault detection for conveyor idlers with 98.7% accuracy and low power consumption.

Despite these advances, challenges persist in environmental noise robustness, weak signal identification under low SNR conditions, and scalable real-time processing in practical deployments. Future developments are expected to focus on several key directions: frequency-comb-enhanced DAS for ultra-sensitive sensing, integrated sensing and communication architectures for improved resource utilization, and embedded AI chips for real-time massive data processing. Additional priorities will include distributed amplification for extending the sensing range, multi-parameter hybrid sensing (acoustic, temperature, and strain), and standardization efforts to ensure interoperability and deployment efficiency.

Through continued advances in new photonic devices, AI edge processing, and system optimization, the DAS is positioned to become a core sensing technology for environmental monitoring and industrial automation in smart cities, driving a paradigm shift toward safer, more efficient, and sustainable infrastructures worldwide.

Declarations

Conflict of Interest The authors declare that they have no competing interests.

Permissions All the included figures, tables, or text passages that have already been published elsewhere have obtained the permission from the copyright owner(s) for both the print and online format.

Use of AI Statement None.

References

[1] I. Ashry, Y. Mao, B. Wang, F. Hveding, A. Y. Bukhamsin, T. K. Ng, *et al.*, "A review of distributed fiber-optic sensing in the oil and gas industry," *Journal of Lightwave Technology*, 2022, 40(5): 1407–1431.

[2] Y. Rao, Z. Wang, H. Wu, Z. Ran, and B. Han, "Recent advances in phase-sensitive optical time domain reflectometry (*Φ*-OTDR)," *Photonic Sensors*, 2021, 11(1): 1–30.

[3] Z. He and Q. Liu, "Optical fiber distributed acoustic sensors: a review," *Journal of Lightwave Technology*, 2021, 39(12): 3671–3686.

[4] S. Liu, F. Yu, R. Hong, W. Xu, L. Shao, and F. Wang, "Advances in phase-sensitive optical time-domain reflectometry," *Opto-Electronic Advances*, 2022, 5(3): 200078.

[5] H. Zhu, W. Liu, T. Wang, J. Su, and B. Shi, "Distributed acoustic sensing for monitoring linear infrastructures: current status and trends," *Sensors*, 2022, 22(19): 7550.

[6] Z. Wang, B. Lu, Q. Ye, and H. Cai, "Recent progress in distributed fiber acoustic sensing with *Φ*-OTDR," *Sensors*, 2020, 20(22): 6594.

[7] M. Arifur Rahman, H. Taheri, F. Dababneh, S. Sattarpanah Karganroudi, and S. Arhamnamazi, "A review of distributed acoustic sensing applications for railroad condition monitoring," *Mechanical Systems and Signal Processing*, 2024, 208: 110983.

[8] S. Li, R. Peng, and Z. Liu, "A surveillance system for urban buried pipeline subject to third-party threats based on fiber optic sensing and convolutional neural network," *Structural Health Monitoring*, 2021, 20(4): 1704–1715.

[9] Y. Wu, L. Gao, J. Chai, Z. Li, C. Ma, F. Qiu, *et al.*, "Overview of health-monitoring technology for long-distance transportation pipeline and progress in DAS technology application," *Sensors*, 2024 24(2): 413.

[10] C. Han, Y. Dong, S. Qu, L. Dong, C. Zhao, A. Madan, *et al.*, "A semi-supervised diffusion-based paradigm for vehicle-track system health monitoring with distributed acoustic sensing," *IEEE Transactions on Intelligent Transportation Systems*, 2025, 26(11): 19381–19397.

[11] Y. Bai, T. Lin, and Z. Zhong, "Noise reduction method of *Φ*-OTDR system based on EMD-TFPF algorithm," *IEEE Sensors Journal*, 2021, 21(21): 24084–24089.

[12] M. Wu, Y. Chen, P. Zhu, and W. Chen, "NLM parameter optimization for *Φ*-OTDR signal," *Journal of Lightwave Technology*, 2021, 40(17): 6045–6051.

[13] J. Zhang, Y. Yan, S. Liu, X. Chen, A. P. T. Lau, C. Yu, *et al.*, "Adaptive block-matching and 3D denoising for *Φ*-OTDR under ultra-low SNR conditions," *Journal of Lightwave Technology*, 2024, 42(13): 4698–4705.

[14] S. Li, K. Liu, J. Jiang, T. Xu, Z. Ding, Z. Sun, *et al.*, "An ameliorated denoising scheme based on deep learning for *Φ*-OTDR system with 41-km detection range," *IEEE Sensors Journal*, 2022, 22(20): 19666–19674.

[15] F. Peng, X. Zheng, and Q. Miao, "Large dynamic range and anti-fading phase-sensitive OTDR using 2D phase unwrapping via neural network," *IEEE Transactions on Instrumentation and Measurement*, 2024, 72: 7006908.

[16] D. F. Kandamali, X. Cao, M. Tian, M. Tian, Z. Jin, H. Dong, *et al.*, "Machine learning methods for identification and classification of events in *Φ*-OTDR systems: a review," *Applied Optics*, 2022, 61(11): 2975–2997.

[17] Y. Wang, P. Tovar, M. C. Dumouchel, L. Chen, X. Bao, "Distributed phase-matching measurement enabled dynamic temperature-strain discrimination using single chirped pulse probe," *APL Photonics*, 2024 9(10): 106118.

[18] X. Zhou, F. Wang, C. Yang, Z. Zhang, Y. Zhang,

and X. Zhang, "Hybrid distributed optical fiber sensor for the multi-parameter measurements," *Sensors*, 2023, 23(16): 7116.
[19] Y. Rao, Z. Ran, and K. Xie, "Performance enhancement of a distributed optical fiber sensing system using a subcarrier technique," Chinese Patent ZL200710048376.X, Sept. 9, 2009.
[20] J. Muir and Z. Zhan, "Seismic wavefield reconstruction using a pre-conditioned wavelet-curvelet compressive sensing approach." *Geophysical Journal International*, 2021, 227(1): 303–315.
[21] F. Jiang, H. Li, Z. Zhang, Z. Hu, Y. Hu, Y. Zhang, *et al.*, "Undersampling for fiber distributed acoustic sensing based on coherent phase-OTDR," *Optics Letters*, 2019, 44(4): 911–914.
[22] F. Yu, S. Liu, L. Shao, W. Xu, D. Xiao, F. Zhao, *et al.*, "Ultra-low sampling resolution technique for heterodyne phase-OTDR based distributed acoustic sensing," *Optics Letters*, 2022, 47(14): 3379–3382.
[23] L. Shao, J. Zhang, X. Chen, D. Xu, H. Gu, F. Yu, *et al.*, "Artificial intelligence-driven distributed acoustic sensing technology and engineering application," *PhotoniX*, 2025, 6(1): 4.
[24] L. Xie, M. Wu, Z. Li, W. Zhou, Y. Rao, and Y. Wu, "Optical fiber distributed acoustic sensing based on difference-frequency COTDR," in *Asia-Pacific Optical Sensors Conference*, Tianjin, China, June 12–16, 2023, pp. 36–38.
[25] L. Xiao, Y. Wang, Y. Li, Q. Bai, X. Liu, and B. Jin, "Polarization fading suppression for optical fiber sensing: a review," *IEEE Sensors Journal*, 2022, 22(9): 8295–8312.
[26] Z. Qin, T. Zhu, L. Chen, and X. Bao, "High sensitivity distributed vibration sensor based on polarization-maintaining configurations of phase-OTDR," *IEEE Photonics Technology Letters*, 2011, 23(15): 1091–1093.
[27] L. Wang, Z. Lin, Z. Cheng, L. Lu, Y. Wang, J. Wang, *et al.*, "Interference fading free *Φ*-OTDR using dual polarization multi-subcarrier LFM signals with MIMO in fractional domain," *Journal of Lightwave Technology*, 2024, 42(18): 6501–6510.
[28] H. Li, T. Liu, C. Fan, B. Yan, J. Chen, T. Huang, *et al.*, "Fading suppression for distributed acoustic sensing assisted with dual-laser system and differential-vector-sum algorithm," *IEEE Sensors Journal*, 2022, 22(10): 9417–9425.
[29] J. Zhou, Z. Pan, Q. Ye, H. Cai, R. Qu, and Z. Fang, "Characteristics and explanations of interference fading of a *Φ*-OTDR with a multi-frequency source," *Journal of Lightwave Technology*, 2013, 31(17): 2947–2954.
[30] X. Pan, K. Cui, A. Zheng, Z. Ren, J. Ma, and R. Zhu, "Fading suppression method based on redundant data within the spatial resolution and deep learning for a *Φ*-OTDR system," *Optics Express*, 2025, 33(9): 18642–18658.
[31] F. Jiang, Z. Zhang, Z. Lu, H. Li, Y. Tian, Y. Zhang, *et al.*, "High-fidelity acoustic signal enhancement for phase-OTDR using supervised learning," *Optics Express*, 2021, 29(21): 33467–33480.
[32] L. Xie, M. Wu, Y. Wang, J. Bai, Y. Rao, and Y. Wu, "Fading suppression of distributed acoustic sensing systems based on polarization-multifrequency diversity fusion," in *28th International Conference on Optical Fiber Sensors*, Shizuoka, Japan, Nov. 20–24, 2023, pp.Tu3–2.
[33] M. Ren, P. Lu, L. Chen, and X. Bao, "Theoretical and experimental analysis of *Φ*-OTDR based on polarization diversity detection," *IEEE Photonics Technology Letters*, 2016, 28(6): 697–700.
[34] D. Chen, Q. Liu, and Z. He, "Phase-detection distributed fiber-optic vibration sensor without fading-noise based on time-gated digital OFDR," *Optics Express*, 2017, 25(7): 8315–8325.
[35] Y. Wu, Z. Wang, J. Xiong, J. Jiang, S. Lin, and Y. Chen, "Interference fading elimination with single rectangular pulse in *Φ*-OTDR," *Journal of Lightwave Technology*, 2019, 37(13): 3381–3387.
[36] H. Qian, B. Luo, H. He, Y. Zhou, C. Hu, X. Zou, *et al.*, "Fading-free *Φ*-OTDR with multi-frequency decomposition," *IEEE Sensors Journal*, 2022, 22(3): 2160–2166.
[37] M. Zhang, Y. Li, Y. Zhao, and Y. Wang, "A dual attention denoising network for DAS VSP signal recovery and its interpretability analysis," *IEEE Transactions on Geoscience and Remote Sensing*, 2024, 62: 5902915.
[38] J. Tejedor, J. Gonzalez-Herraez, H. Martins, J. Pastor-Graells, S. Martín-López, P. Corredera Guillén, *et al.*, "Real field deployment of a smart fiber-optic surveillance system for pipeline integrity threat detection: architectural issues and blind field test results," *Journal of Lightwave Technology*, 2018, 36(4): 1052–1062.
[39] H. Wu, X. Liu, Y. Xiao, and Y. Rao, "A dynamic time sequence recognition and knowledge mining method based on the hidden Markov models (HMMs) for pipeline safety monitoring with *Φ*-OTDR," *Journal of Lightwave Technology*, 2019, 37(19): 4991–5000.
[40] S. Shi, Z. Han, Z. Liu, P. Vallely, S. Soua, S. Kaewunruen, *et al.*, "Quantitative monitoring of brittle fatigue crack growth in railway steel using acoustic emission," *Proceedings of the Institution of Mechanical Engineers*, 2018, 232(4): 1211–1224.
[41] K. Tiwari, R. Raisutis, O. Tumsys, A. Ostreika, K. Jankauskas, and J. Jakutavicius, "Defect estimation in non-destructive testing of composites by ultrasonic guided wave and image processing," *Electronics*, 2019, 8(3): 315.
[42] F. Hernandez-Valle, A. R. Clough, and R. S. Edwards, "Stress corrosion cracking detection using non-contact ultrasonic techniques," *Corrosion*

Science, 2014, 78: 335–342.

[43] S. Han, S. Cho, G. Jang, and J. Park, "Non-contact inspection of rail surface and internal defects based on electromagnetic ultrasonic transducers," *Journal of Intelligent Material Systems and Structures*, 2016, 27(3): 427–434.

[44] Y. Jia, K. Liang, P. Wang, K. Ji, and P. Xu, "Enhancement method of magnetic flux leakage signals for rail track surface defect detection," *IET Science, Measurement & Technology*, 2020, 14(6): 711–717.

[45] F. Peng, N. Duan, Y. Rao, and J. Li, "Real-time position and speed monitoring of trains using phase-sensitive OTDR," *IEEE Photonics Technology Letters*, 2014, 26(20): 2055–2057.

[46] M. He, L. Feng, and D. Zhao, "Application of distributed acoustic sensor technology in train running condition monitoring of the heavy-haul railway," *Optik*, 2019, 181: 343–350.

[47] A. Wagner, A. Nash, F. Michelberger, H. Grossberger, and G. Lancaster, "The effectiveness of distributed acoustic sensing (DAS) for broken rail detection," *Energies*, 2023, 16(1): 522.

[48] L. Xie, Z. Li, Y. Zhou, W. Xiang, Y. Wu, and Y. Rao, "Railway track online detection based on optical fiber distributed large-range acoustic sensing," *IEEE Internet of Things Journal*, 2024, 11(4): 6469–6480.

[49] A. Masoudi, M. Belal, and T. P. Newson, "A distributed optical fibre dynamic strain sensor based on phase-OTDR," *Measurement Science and Technology*, 2013, 24(8): 085204.

[50] C. Fan, H. Li, B. Yan, Y. Sun, T. He, T. Huang, *et al.*, "High-precision distributed detection of rail defects by tracking the acoustic propagation waves," *Optics Express*, 2022, 30(22): 39283–39293.

[51] D. P. Connolly, G. Kouroussis, O. Laghrouche, C. L. Ho, and M. C. Forde, "Benchmarking railway vibrations-track, vehicle, ground and building effects," *Construction and Building Materials*, 2015, 92: 64–81.

[52] L. Xu and W. Zhai, "A novel model for determining the amplitude-wavelength limits of track irregularities accompanied by a reliability assessment in railway vehicle-track dynamics," *Mechanical Systems and Signal Processing*, 2017, 86: 260–277.

[53] S. Kowarik, M. T. Hussels, S. Chruscicki, S. Munzenberger, A. Lämmerhirt, P. Pohl, *et al.*, "Fiber optic train monitoring with distributed acoustic sensing: conventional and neural network data analysis," *Sensors*, 2020, 20(2): 450.

[54] F. Peng, Z. Zhu, Y. Zhang, and Q. Miao, "A deep learning image segmentation model for detection of weak vehicle-generated quasi-static strain in distributed acoustic sensing," *IEEE Transactions on Intelligent Transportation Systems*, 2025, 26(6): 8933–8944.

[55] H. Wu, X. Wang, P. Zhang, Y. Zhao, J. Jiang, L. Xie, *et al.*, "High precision railfusion-DAS for railway track defect detection using existing communication fibers," *Optics Express*, 2025, 33(20): 42928–42946.

[56] A. Roohezamin, R. Kalatehjari, M. Hajihassani, M. Kharghani, and D. Dias, "Investigation of acoustic waves behavior of an underground tunnel in a multilayer soil," *Scientific Reports*, 2022 12: 13399.

[57] N. Harmon, C. A. Rychert, J. Davis, G. Brambilla, W. Buffet, B. Chichester, *et al.*, "Surface deployment of DAS systems: coupling strategies and comparisons to geophone data," *Near Surface Geophysics*, 2022, 20(5): 465–477.

[58] Y. Wang, W. Chang, J. Li, and C. Yang, "Signal processing for enhancing railway communication by integrating deep learning and adaptive equalization techniques," *PLOS One*, 2024, 19(10): e0311897.

[59] E. Uygun and S. Terzi. "Acoustic monitoring of railway defects using deep learning with audio to spectrogram conversion," *Journal of Vibration Engineering & Technologies*, 2024, 12(2): 2585–2594.

[60] D. Miao, Y. Wang, and S. Li, "Sound-based improved DenseNet conveyor belt longitudinal tear detection," *IEEE Access*, 2022, 10: 123801–123808.

[61] D. He, X. Liu, and B. Zhong. "Sustainable belt conveyor operation by active speed control," *Measurement*, 2020, 154: 107458.

[62] H. Wijaya, P. Rajeev, E. Gad, and R. Vivekanantham, "Automatic fault detection system for mining conveyor using distributed acoustic sensor," *Measurement*, 2022, 187: 110330.

[63] Y. Liu, Y. Wu, X. Jiao, X. Li, H. Wu, and J. Zhou, "Rapid edge-computing for intelligent fiber-optic DAS," *IEEE Sensors Journal*, 2025, 25(10): 17062–17071.